Computers in Biology and Medicine 115 (2019) 103481

Contents lists available at ScienceDirect

Computers in Biology and Medicine

journal homepage: http://www.elsevier.com/locate/compbiomed

Negative binomial maximum likelihood expectation maximization (NB-MLEM) algorithm for reconstruction of pre-corrected PET data

Michele Scipioni [a,b], Maria Filomena Santarelli [b,c,*], Assuero Giorgetti [c], Vincenzo Positano [c], Luigi Landini [a,c]

[a] Dipartimento di Ingegneria dell'Informazione, University of Pisa, Pisa, Italy
[b] CNR Institute of Clinical Physiology, Via Moruzzi,1, 56124, Pisa, Italy
[c] Fondazione Toscana "G. Monasterio", Via Moruzzi,1, 56124, Pisa, Italy

ARTICLE INFO

Keywords:
PET
Image reconstruction
Pre-corrected PET data
Negative binomial
Maximum likelihood expectation maximization

ABSTRACT

Purpose: Positron emission tomography (PET) image reconstruction is usually performed using maximum likelihood (ML) iterative reconstruction methods, under the assumption of Poisson distributed data. Pre-correcting raw measured counts, this assumption is no longer realistic. The goal of this work is to develop a reconstruction algorithm based on the Negative Binomial (NB) distribution, which can generalize over the Poisson distribution in case of over-dispersion of raw data, that may occur if sinogram pre-correction is used.

Methods: The mathematical derivation of a Negative Binomial Maximum Likelihood Expectation-Maximization (NB-MLEM) algorithm is presented. A simulation study to compare the performance of the proposed NB-MLEM algorithm with respect to a Poisson-based MLEM (P-MLEM) method was performed, in reconstructing PET data. The proposed NB-MLEM reconstruction was tested on a real phantom and human brain data.

Results: For the property of NB distribution, it is a generalization of the conventional P-MLEM: for not over dispersed data, the proposed NB-MLEM algorithm behaves like the conventional P-MLEM; for over-dispersed PET data, the additional evaluation of the dispersion parameter after each reconstruction iteration leads to a more accurate final image with respect to P-MLEM.

Conclusions: A novel approach for PET image reconstruction from pre-corrected data has been developed, which exhibits a statistical behavior that deviates from the Poisson distribution. Simulation study and preliminary tests on real data showed how the NB-MLEM algorithm, being able to explain the over-dispersion of pre-corrected data, can outperform other algorithms that assume no over-dispersion of pre-corrected data, while still not accounting for the presence of negative data, such as P-MLEM.

1. Introduction

In positron emission tomography (PET), image reconstruction is usually performed using iterative reconstruction methods, which use a forward model to account for the Poisson statistics of the measured data and are based on maximum likelihood (ML) optimization. The most popular algorithms are ML Expectation Maximization (MLEM) [1,2] and its accelerated version called Ordered Subsets Expectation Maximization (OSEM) [3].

However, the assumption that the data are Poisson distributed is not always verified, and deviations may occur as a consequence of many causes, mainly the correction of some unwanted physical and acquisition artefacts, such as: scattered or accidental counts, positron range, dead-time, photon non-co-linearity, variation in detector-pair sensitivity, and others [4–10].

Accidental (random) coincidences add wrong additional counts to LORs in the sinogram, which cause a reduced contrast and an overestimation of the tracer activity [11]. Random events cause a reduction of image contrast and a bias in the measured activity due to an increased level of background activity [12]. Usually, PET scanners detect coincidences both during 'prompt' and 'delayed' time windows. Prompt coincidences represent true coincidences, corrupted by random and scatter events, while delayed coincidences represent only random events.

Modern PET scanners use EM-based reconstruction algorithms that preserve the Poisson nature of the data, including into the

* Corresponding author. CNR Institute of Clinical Physiology, Via Moruzzi,1, 56124, Pisa Italy.
E-mail address: mariafilomena.santarelli@cnr.it (M.F. Santarelli).

https://doi.org/10.1016/j.compbiomed.2019.103481
Received 26 March 2019; Received in revised form 1 October 2019; Accepted 1 October 2019
Available online 2 October 2019

reconstruction process all the factors that may alter the statistical distribution of the data [13,14]: the scatter and random estimates, finite resolution model, irregularities in the geometry, etc. This has the advantage of maintaining the Poisson statistic of the data.

An alternative method is that of pre-correcting data before reconstruction. In this case, a common strategy to correct for accidental coincidences is to subtract the delayed (noisy) coincidences from the total events [15], leading to an overdispersion of data; such overdispersion is stronger when the noisy estimate of the accidentals is uncorrelated with the measurement noise. Scatter correction is usually performed after random correction. Different methods for correcting scattering effects exist [7]: the simplest one is based on the assumption that we can approximate the distribution of scattered coincidences by fitting a Gaussian function to each projection profile in the sinogram; more accurate methods, such as the single-scatter simulation [16] (SSS), consist of an estimate of scattered events distribution using information from the total sinogram and from computer modelling of the photon interaction physics. By correcting raw measured counts for these effects, the assumption of Poisson-distributed data is no longer realistic [13]. Depending on how much the newly corrected sinogram deviates from a Poisson statistic, this may compromise the estimation of the emission density.

A viable approach to noise and bias reduction may be to identify an optimal way to model the deviation from the Poisson statistic in pre-corrected count data and to exploit this information in PET image reconstruction. A reasonable way may be provided by the Negative Binomial (NB) distribution, which is able to model count data with different degrees of dispersion, in particular when the variance exceeds the mean value (i.e. over-dispersion) [9,17–20]. The authors of this work previously demonstrated [9] that PET data after random and accidental scattering correction are no longer Poisson distributed but they present an over-dispersion of data, and therefore they can be better modeled using an NB distribution. This was demonstrated also for a real phantom data. Furthermore, this over-dispersion is still present after applying all corrections [10] (i.e. random scattering, dead time, normalization, geometric, accidental scattering, and attenuation), and therefore, an NB distribution is well suited to characterize these pre-corrected PET data.

It is known that an ML estimator based on the correct statistical model is asymptotically efficient (lowest possible variance), so modifying the log-likelihood with the suitable model, may lead to solutions with lower bias and variance. The aim of this work is reducing the bias and the variance observed in PET reconstructed images by using the appropriate statistics of data (i.e. NB instead of Poisson); it is especially relevant when dealing with low counts acquisitions, which may occur when a low dose of radiotracer is injected into the patient body or when the aim is to lower the acquisition time, i.e. to increase time resolution in dynamic scans.

In this work, the mathematical derivation of an NB-based MLEM reconstruction algorithm is presented. A simulation study and preliminary tests on a real phantom and human brain data showed how this algorithm could be efficiently used to reconstruct pre-corrected PET data, reducing bias and variance on the resulting images with respect to a Poisson-based MLEM.

2. Materials and methods

2.1. The NB distribution model

The NB distribution can be seen as a generalization of the Poisson distribution, which is able to describe count data with different degrees of over-dispersion, including the special case of variance equal to mean value, typical of Poisson distribution. NB distribution is a function of two parameters: the mean $\lambda$and the r factor [9,17]:

$$p(Y=y;\lambda,r)=NegBin(Y=y|\lambda,r)=\frac{\Gamma(y+r)}{\Gamma(y+1)\cdot\Gamma(r)}\left(\frac{r}{\lambda+r}\right)^{r}\left(\frac{\lambda}{\lambda+r}\right)^{y},\ \lambda>0\ ,\ r>0 \tag{1}$$

where $\Gamma(\cdot)$ is the gamma function, and y is a non-negative integer value.

Eq. (1) represents the probability density function (*pdf*) of the NB distribution. The parameter r is important to characterize the deviation from a Poisson distribution. Sometimes the inverse of the r parameter, $\alpha = 1/r$, is used to quantify the over-dispersion of the samples $y = \{y_i\}$, with respect to the mean value of the *pdf*. The mean of the NB distribution is λ (as for the Poisson distribution) and, using the method of moments [20], the variance σ^2 is:

$$\sigma^2=\lambda(1+\alpha\lambda) \tag{2}$$

As α gets small with respect to λ, the NB distribution converges to a Poisson distribution, being $\sigma^2=\lambda$ for $\alpha = 0$.

2.2. The log-likelihood for NB distribution

The derivation of an MLEM reconstruction algorithm based on the hypothesis of NB distributed data follows closely the reasoning behind the derivation of the original Poisson-based algorithm (P-MLEM). Let the radiotracer activity within the patient's body be a continuous function $\tilde{x}$, which can be discretized using a set of point sources $x = \{x_j\}$, $j \in \{1,\ldots,J\}$. Each voxel emits radiation at an average rate of x_j proportional to local tracer concentration. The geometry of the acquisition system and the attenuation determine the probability p_{ij} of a photon emitted by voxel j being detected by Line of Response (LOR) i. Let $\tilde{y}$ be the raw measured projection data, which are usually described as a Poisson random variable, with expected value $\lambda_i = \lambda_i(x) = \sum_j p_{ij}x_j$. The correction of artefacts causes a change in the statistical distribution of the projection data, with a transition from Poisson to Negative Binomial [9].

Let $y = \{y_i\},\ \ i \in \{1,\ldots,I\}$ represent the pre-corrected projection counts stored as a sinogram. Given the activity x, then, the probability to observe counts y_i in detector bin i can be modeled as:

$$p(y_i|\lambda_i,r)=NegBin\left(Y=y_i|\ \lambda_i(x)=\sum_j p_{ij}x_j,\ \ r\right) \tag{3}$$

It follows that counts in each detector bin i are independent, conditionally to the activity x, and thus the probability of observing y given x is:

$$p(y|\lambda(x),r)=\prod_i p(y_i|\lambda_i(x),r) \tag{4}$$

Eq. (4) is the likelihood of observing the pre-corrected projection measurement, given an emission activity x and a parameter r. It is useful to express the likelihood in logarithmic form to simplify the calculus of derivatives in the following steps:

$$\begin{aligned} l(x,r) &= \log\left(\ p\left(y|\ \lambda(x)=\sum_j p_{ij}x_j,r\right)\ \right) \\ &= \sum_i\Big[\log(\Gamma(y_i+r))-\log(\Gamma(y_i+1)) \\ &\quad +\log(\Gamma(r))+r\log(r)+y_i\log\left(\sum_j p_{ij}x_j\right)-(y_i+r)\log\left(r+\sum_j p_{ij}x_j\right)\Big] \end{aligned} \tag{5}$$

2.3. The NB-MLEM iterative algorithm

The conventional approach to iterative statistical image reconstruction is then based on deriving an estimate of the activity image x, so that

the measured photon counts y are more likely to be observed. This means that it is necessary to maximize the log-likelihood function in eq. (5). The problem with the Negative Binomial distribution is that eq. (5) is a function of two parameters, and it is necessary to estimate both, instead of just computing the expectation of the mean value $\lambda(x)$.

2.3.1. Updating the estimate of the mean value x

An update formula for the activity image x can be derived following similar reasoning used by Shepp and Vardi [1] and Lange and Carson [2] for Poisson distributed emission tomography data. The estimate of the activity spatial distribution can be computed minimizing the negative of the log-likelihood in eq. (5) with respect to x, under the positivity constraint $x \geq 0$. As this minimization problem is convex [21], it is possible to make use of results from convex analysis to find a global minimum of x. The first step foresees to compute the partial derivative of (5) with respect to the activity x:

$$\frac{\partial l(x,r)}{\partial x_j} = \sum_i \left[-p_{ij} \frac{1+\alpha\, y_i}{1+\alpha \sum_j p_{ij} x_j} + p_{ij} \frac{y_i}{\sum_j p_{ij} x_j} \right] \tag{6}$$

where $\alpha = 1/r$ was used for the sake of clarity of the notation.

Formally, the Karush-Kuhn-Tucker (KKT) conditions [22] provide the existence of a Lagrange multiplier function $v \geq 0$, such that the stationary points of eq. (6) satisfy equations:

$$0 = -\frac{\partial l(x,r)}{\partial x_j}\bigg|_{\widehat{x}_{j,ML}} - v = \sum_i \left[p_{ij} \frac{1+\alpha\, y_i}{1+\alpha \sum_j p_{ij} x_j} - p_{ij} \frac{y_i}{\sum_j p_{ij} x_j} \right]\bigg|_{\widehat{x}_{j,ML}} - v \tag{7.a}$$

$$0 = v\, x_j \big|_{\widehat{x}_{j,ML}} \tag{7.b}$$

Eq. (7.a) is the first order optimality condition and, without loss of generality, it can be rewritten as:

$$\sum_i \left[1_X - \frac{1}{p_{ij} \frac{1+\alpha\, y_i}{1+\alpha \sum_j p_{ij} x_j}} p_{ij} \frac{y_i}{\sum_j p_{ij} x_j} \right] - \frac{v}{p_{ij} \frac{1+\alpha\, y_i}{1+\alpha \sum_j p_{ij} x_j}} = 0 \tag{8}$$

Since the optimization problem is convex, every solution $\widehat{x}$ satisfying $\widehat{x} \geq 0$ and the two KKT conditions is a global minimizer. If that is the case, $\widehat{x}$ is a fixed stationary point of the optimization and it is possible to approximate the constant term 1_X in eq. (8) by $\frac{\widehat{x}_j^{(n+1)}}{\widehat{x}_j^{(n)}}$ such that $\widehat{x}_j^{(n+1)}$ appears directly:

$$\widehat{x}_j^{(n+1)} - \widehat{x}_j^{(n)} \sum_i \left[\frac{1}{p_{ij} \frac{1+\alpha\, y_i}{1+\alpha \sum_j p_{ij} x_j}} p_{ij} \frac{y_i}{\sum_j p_{ij} x_j} \right] - \frac{v \widehat{x}_j^{(n)}}{p_{ij} \frac{1+\alpha\, y_i}{1+\alpha \sum_j p_{ij} x_j}} = 0 \tag{9}$$

The last term in eq. (9) can be eliminated according to eq. (7.b), and by straightforward reordering a simple, fixed point, iteration scheme is obtained, for the update of the activity image estimate:

$$\widehat{x}_j^{(n+1)} = \widehat{x}_j^{(n)} \frac{1}{\sum_i p_{ij} \frac{1+\alpha\, y_i}{1+\alpha \sum_h p_{ih} \widehat{x}_h^{(n)}}} \sum_i p_{ij} \frac{y_i}{\sum_k p_{ik} \widehat{x}_k^{(n)}} \tag{10}$$

which preserves non-negativity if the operator p_{ij} preserves non-negativity and the initialization $x^{(0)}$ is non-negative [23]. Eq. (10) is the maximum likelihood expectation maximization in case of NB-distributed counts data (NB-MLEM), and it allows to iteratively update the estimate of the activity image x, given the knowledge of pre-corrected measured counts y, and data dispersion factor $\alpha = 1/r$. It is straightforward to see that eq. (10) is a generalization of the Poisson MLEM (P-MLEM) conventionally used in emission tomography iterative image reconstruction, as it converges to P-MLEM for $\alpha \to 0$ (i.e. the same condition under which a NB distribution converges to a Poisson distribution).

2.3.2. Updating the estimate of the parameter r

Eq. (10) can be used to estimate the activity image from count projection, only if the value of the parameter r is known. Given that this is never the case, unless it is accepted to approximate the data as, e.g., Poisson distributed with $\alpha = 0$, it is required to alternate between the update of the estimate of the mean value of the NB distribution $\bar{y}_i = \lambda(x)$, and the estimate of the parameter $r = 1/\alpha$.

It is necessary to compute again the derivative of the log-likelihood in eq. (5) with respect to parameter r:

$$\frac{\partial l(x,r)}{\partial r} = \sum_i \left[\sum_{v=0}^{y_i-1} \frac{rv}{r+v} + r^2 \log\left(1 + \frac{\sum_j p_{ij} x_j}{r}\right) - (y_i + r) \frac{\sum_j p_{ij} x_j}{1 + \frac{\sum_j p_{ij} x_j}{r}} \right] \tag{11}$$

Using eq. (11) to derive a closed-form iterative solution to find a value $\widehat{r} = argmax_r\, l(x,r)$ is not trivial [24]. For this reason, it was chosen to approximate the ML update of the value of the r parameter using numeric approximations. In this work, a random search approach based on the direct sampling of the likelihood function was adopted:

1. Given the current estimate of the activity $\widehat{x}^{(n)}$, from eq. (10), random samples of r is drawn from a uniform distribution on a predefined search space to compute an approximation $\widehat{l}(\widehat{x}^{(n)}, r)$ of the log-likelihood function in eq. (5), as a function of r;
2. The value $\widehat{r}_m = argmax_r\ \widehat{l}(\widehat{x}^{(n)}, r)$ is chosen as the one yielding the maximum value of $\widehat{l}(\widehat{x}^{(n)}, r)$;
3. Steps 1 and 2 are repeated M times, adapting the search space according to the current estimate $\widehat{r}_m$;
4. In the end, the new value of the r parameter for the n-th reconstruction iteration is chosen as:

$$\begin{cases} \widehat{r}^{(n)} = argmax_{\widehat{r}_m}\, \widehat{l}\left(\widehat{x}^{(n)}, \widehat{r}_m\right), \quad m = 1, \ldots, M \\ \widehat{\alpha}^{(n)} = \dfrac{1}{\widehat{r}^{(n)}} \end{cases} \tag{12}$$

2.3.3. Summary of the algorithm and implementation details

The NB-MLEM algorithm, therefore, consists of updating, at each iteration, the values of $\widehat{x}_j^{(n+1)}$ according to eq. (10), and $\widehat{r}^{(n+1)}$ (and then $\widehat{\alpha}^{(n+1)}$) according to eq. (12). The flowchart in Fig. 1 summarizes the entire process: starting from a blank initialization guess ($\widehat{x}^{(0)}$), the NB-MLEM algorithm iteratively updates the estimate of activity image ($\widehat{x}^{(n+1)}$) using eq. (10) for a given value of the dispersion factor $\widehat{\alpha}$. This update, then, produces a new estimate ($\widehat{y}^{(n)} = \lambda(\widehat{x}^{(n)}) = \sum_j p_{ij} \widehat{x}_j^{(n)}$) of the pre-corrected sinogram (y) via forward projection. On the estimated counts, a new value for the parameter ($\widehat{r}^{(n)}$) is computed as described in section 2.3.2. Fig. 1 also shows a few examples of how successive iterations change the estimates of activity images and sinogram expectations; also the NB log-likelihood is shown as a function of the parameter r, and we can see how it changes its shape with successive iterations, with its maximum progressively approaching a convergence value.

To ensure the convergence of the algorithm it needs the objective function to be convex; in such case the negative log-likelihood function has a global minimum. Since the NB negative log-likelihood in Eq. (5) is not convex for every value of r and x, in such cases local minima should be found during the algorithm iterations; this can be avoided by using multiple sets of initial conditions of the parameters [25]. In the present work, we used this approach to update the estimate of parameter r by adapting the search space for the random sampling as described in

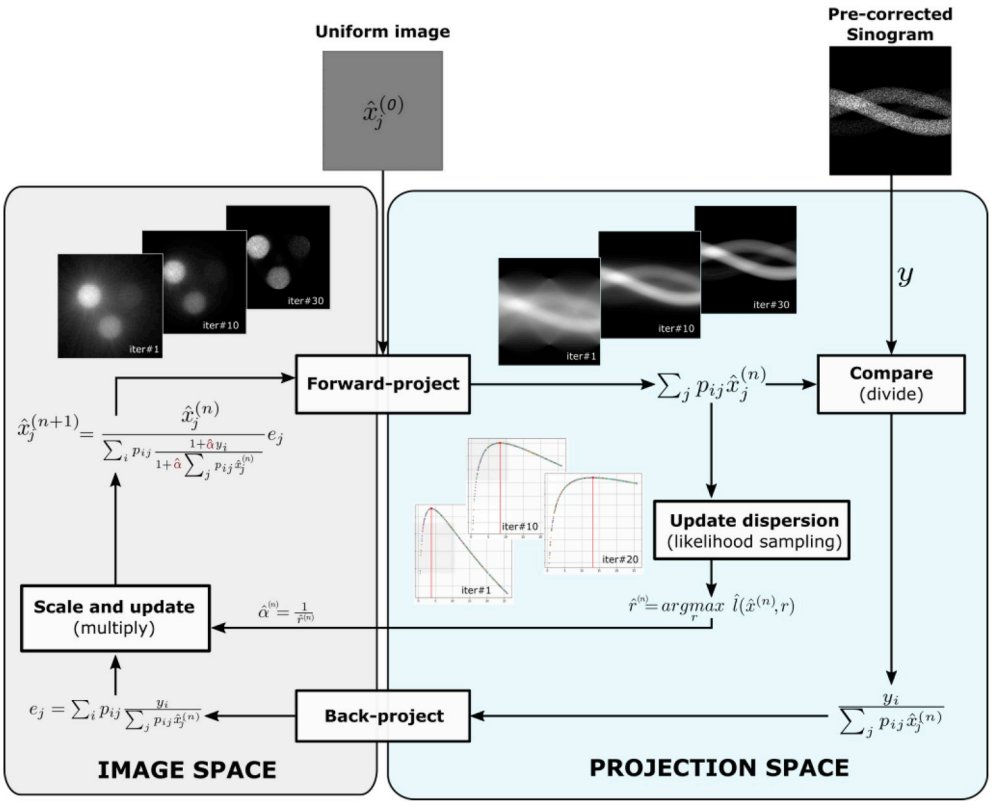

Fig. 1. Flow diagram of the NB-MLEM reconstruction algorithm.

section 2.3.2 in order to try to reduce the risk of finding a local minimum as much as possible.

To implement the NB-MLEM reconstruction algorithm, the in-house-developed software *Occiput.io* [26,27] was used, which exploits GPU parallel computation for the operations of projection and back-projection to speed up the reconstruction process. For the P-MLEM reconstruction that was used as a reference and compared to NB-MLEM, we used the default implementation provided by the *Occiput.io* library.

2.4. Simulation

Static [^{18}F]FDG PET scans were simulated for a Discovery RX VCT (64-slice, GE Healthcare, Milwaukee, WI) PET/CT scanner, using the digital phantom shown in Fig. 2a. It is composed by three cylindrical regions (6 cm × 15 cm, radius x height, each), filled with different tracer concentrations, so to assess the performance of the proposed reconstruction algorithm to recover different tissues' emission. The average emission $\bar{x}_j$ in each region was ~75 Bq/ml, ~40 $Bq/$ml, and 12 Bq/ml, respectively, for a total simulated injected activity in the cylindrical phantom of ~12 MBq Red circles identify the three ROIs used later on to assess the performance of the reconstruction. Four different scan time lengths were simulated, to study the impact of sinogram count rate on reconstruction quality and convergence properties of the NB-MLEM. Scan durations and relevant total number of counts in the projected sinogram are shown in Table 1.

Fig. 2b shows the ideal noiseless sinogram obtained by forward projecting the phantom in Fig. 2a, mimicking an acquisition length of 150s. The chosen scanner geometry is such to store coincidence events on a sinogram grid of 331 × 315 bins. To approximate the NB statistical distribution typical of pre-corrected sinogram data, while having full control on and knowledge of the true values of the parameters to be estimated, NB-distributed data were generated using the noiseless sinogram as mean $\lambda(x)$, and multiple values for the parameter $r = [3.25, 6.5, 13.0, 1e9]$. The last value of $r = 1e9$ was chosen to simulate a *quasi-*

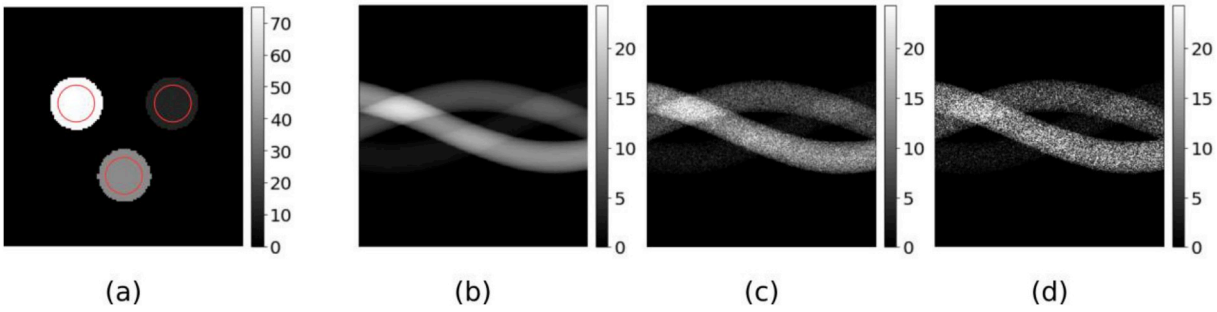

Fig. 2. a) Simulated phantom with three regions with different emission rates (average emission $\bar{x}_j$ in each region is: 75 Bq/ml, 40 Bq/ml, 12 $Bq/\ ml$; red circles identify the three ROIs used later on to assess the performance of the reconstruction: they will be labeled as 'high activity', 'medium activity' and 'low activity', starting from top-left and moving counterclockwise. b) Noiseless sinogram projection (total counts ~*250 kCounts*). c) Example of Poisson-distributed projection data. d) Example of NB-distributed projections data (with $r = 3.25$).

Table 1
Different acquisition lengths simulated, to generate sinograms with different signal-to-noise characteristics.

Acquisition length	150 s	300 s	600 s
Total measured counts (single 2D sinogram slice)	~*250 kCounts*	~*500 kCounts*	~*1000 kCounts*

Poisson condition (i.e. $\alpha \rightarrow 0$).

Random, accidental scattering and other artefacts were not generated, and consequent correction of the sinogram was not performed in the simulation, because the assumption was made that pre-corrected data is NB-distributed, according to what was demonstrated by authors in Ref. [9]. This allowed us to more accurately control the behaviour of the reconstruction algorithm, as the degree of data over-dispersion varies between datasets.

An example of the NB-distributed sinogram (generated from the noiseless one in Fig. 2b) is shown in Fig. 2c for $r = 1e9$, which approximates a quasi-Poisson distribution, and in Fig. 2d for $r = 3.25$.

2.5. Metrics for comparing the results from the two algorithms

The performance of the proposed NB-MLEM reconstruction of pre-corrected sinogram data was evaluated in comparison with a conventional Poisson MLEM (P-MLEM). The total number of reconstruction iterations was 100, for both the algorithms. All the combinations of scan times and dispersion parameters were tested. For each one of them, the comparison of the two reconstruction methods was quantitatively performed computing bias (i.e. agreement with the ground truth simulated activity) and noise (i.e. standard deviation of a uniform region of interest) from the reconstructed images, as follows:

$$bias[\%] = 100 * \left[\frac{1}{N_{roi}} \sum_{j \in ROI} \frac{\left| \hat{x}_j - x_j^{true} \right|}{x_j^{true}} \right] \tag{13}$$

$$noise[a.u.] = \sqrt{\frac{1}{N_{roi}} \sum_{j \in ROI} \left| \hat{x}_j - x_j^{true} \right|^2} \tag{14}$$

Bias and noise were computed, at each reconstruction iteration, on regions of interest relevant to each region of the phantom, as shown in Fig. 2a using red circles.

2.6. Experimental phantom acquisition and reconstruction

A cylindrical phantom (12 cm × 15 cm, radius x height) was filled with 18F-FDG and water solution. The total activity at the beginning of the experiment was of 34MBq. The phantom was placed in the middle of the bore of a PET/CT scanner (Discovery RX VCT 64-slice, GE Healthcare, Milwaukee, WI), with its long axis parallel to the bore's axis. 47 slices of 2D PET data projections covering the phantom were acquired for six different times, with a time interval of about 15–20 min. Each static scan lasted a total time of 300s. The total activity of each static scan ranged from 34MBq to 15MBq. Each static sinogram was treated as a separate scan and corrected, prior to reconstructing, for the following unwanted artefacts: random counts, dead time, normalization, geometric correction, scattering, and attenuation [9]. The sequence of corrections was applied according to the scanner protocol, and the vendor's software was used to compute and apply the relevant correction factors. Sinograms obtained after correction of all artifact were saved for further analysis and image reconstruction, that were performed outside of the scanner workstation, using the software libraries listed in Section 2.3.3.

2.7. Real human brain data acquisition and reconstruction

One dataset of real human brain data was acquired after an injection of ~300*MBq* of [^{18}F]FDG to a subject with no known brain pathology. The same PET/CT scanner used to acquire the phantom was used, and a static scan was performed in 300s, obtaining 47 slices of 2D PET data projections. The vendor software was used to compute all correction matrices, and to pre-correct the measured sinograms using the same procedure previously described for the experimental phantom. Sinograms obtained after correction of all artifact were then reconstructed using both P-MLEM and NB-MLEM.

3. Results

3.1. Simulation results

Fig. 3 shows the reconstructed images at different iteration numbers for the P-MLEM (top row) and NB-MLEM (bottom row) algorithms.

Fig. 4 shows the results obtained in the estimation of the parameter *r*, for all the simulated combinations of total sinogram counts and r parameter. The straight black lines in the graphs indicate the true value of the r parameter in that specific case.

Fig. 5 shows trends of bias (in percentage) vs noise in the reconstructed images, as a function of the iteration number, for increasing values of the parameter *r* (from Fig. 5a–d). In each subfigure, each row presents the abovementioned quality metrics for the three different regions of the phantom, allowing to study different emission rates at once. Fixing the value of the parameter *r* (i.e. one Fig. between Fig. 5a, …,5d) and one region of the phantom (i.e. one of the three columns of which the subfigure is composed), different line styles are used to depict bias vs noise trends for the various scan time lengths simulated.

3.2. Experimental phantom results

In Fig. 6 the results obtained reconstructing the experimental phantom are shown. In particular, Fig. 6a and b shows the reconstructed images acquired at the first (a) and last (b) time points, for different iteration numbers. In both subfigures, in the top row, the images are reconstructed using P-MLEM algorithm, while in bottom row we used the proposed NB-MLEM algorithm. The red circles show the ROIs used later on to produce the graph in Fig. 7. The log-likelihoods evaluated during the reconstruction of the phantom in the two scan times of Fig. 6a and b are also shown, for both NB-MLEM (blue line) and P-MLEM (orange line), respectively. In Fig. 6c the value of the parameter *r* estimated at each iteration by the NB-MLEM algorithm, for each of the six scans of the real phantom is shown.

In Fig. 7, the ROI mean vs ROI noise is shown as function of the iteration number, for all the 6 scans. Different colors were used to differentiate between the 6 scans of the experimental phantom, and two markers were used to distinguish between the results of the P-MLEM (dotted) and NB-MLEM (continuous) algorithms. The ROI used to compute regional mean and standard deviation is shown in Fig. 6. On the right, a zoom of selected regions of the plots (black rectangles in the main plot) is shown for three of the scans.

3.3. Brain data results

In Fig. 8 the results obtained by brain data reconstruction are shown. In Fig. 8a reconstructed images, at different number of iterations are shown, for the P-MLEM (top) and NB-MLEM (bottom) algorithms. In Fig. 8b the log-likelihood of the two algorithms as function of the iteration number are shown; finally, Fig. 8c shows the trend of the mean value vs standard deviation for an ROI covering brain gray-matter, as function the iteration number. The ROI used is shown in Fig. 8a.

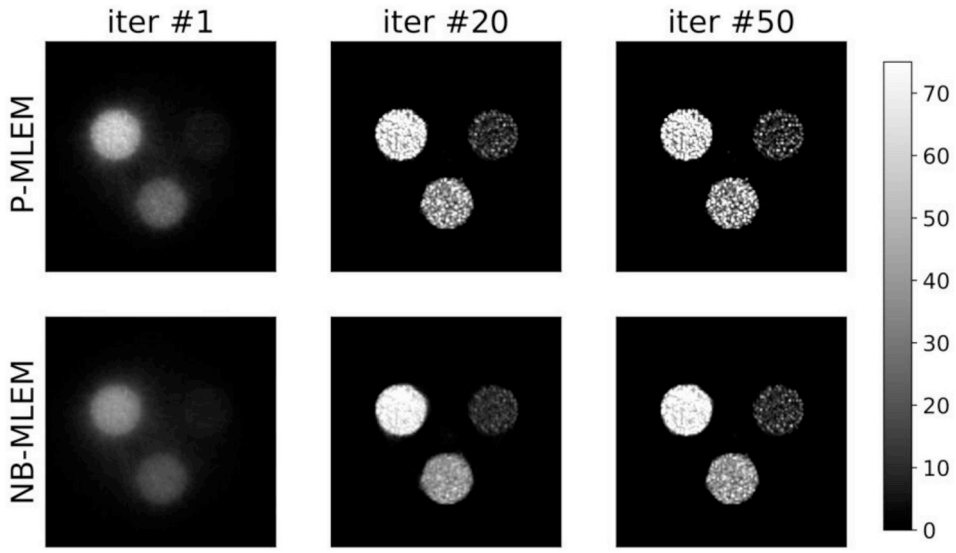

Fig. 3. Reconstructed images at different number of iteration (1,20,50), using P-MLEM (*top row*) and NB-MLEM (*bottom row*), with total sinogram counts per slice of ~2.5*E*5 and a parameter $r = 3.25$.

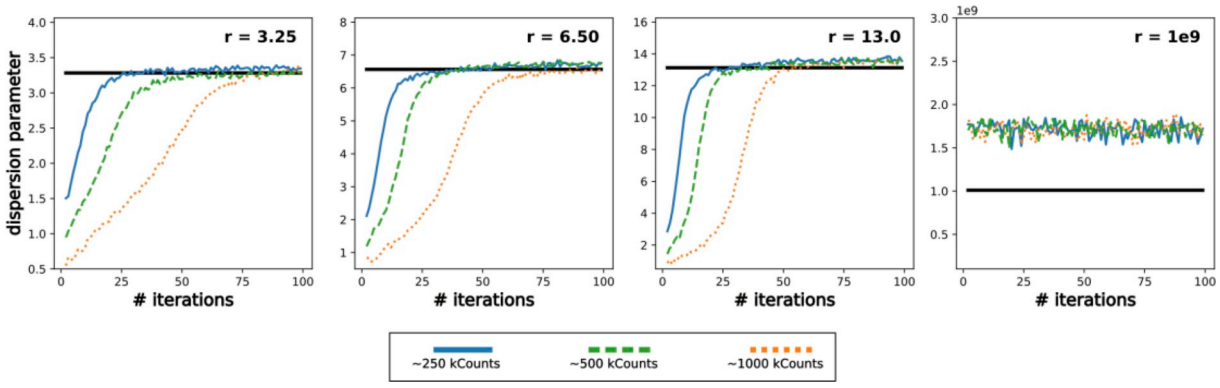

Fig. 4. Parameter r estimation, for different simulated r values: from left to right: $r = 3.25, 6.5, 13.0, 1E9$. In each subfigure, the black line is the reference simulated value, while different line styles and colors describe the behavior of the algorithm under different count rate conditions.

4. Discussion

In this work, the mathematical derivation of an MLEM reconstruction algorithm for pre-corrected PET sinogram data is discussed, under the assumption of modelling the observed data using a Negative Binomial distribution. This research work explores a topic already discussed in the literature about statistical iterative reconstruction, and it could be compared to other methods trying to deal with non-Poisson emission data, using strategies like: approximated Poisson distribution [28], shifted Poisson [29], or Gaussian models [30,31]. The authors of this work previously demonstrated [9,10] that PET data after random and accidental scattering correction are no longer Poisson distributed, and that they present an over-dispersion of data (i.e. variance greater than the mean of the data), and therefore they could be better modeled using an NB distribution.

This modelling choice resulted in the proposal of a reconstruction method, which acts by iteratively updating the estimate of the two parameters of the NB distribution: the mean (which is a function of the activity image x) and the data dispersion factor α(or its dual $r = 1/\alpha$).

In the present work the dispersion factor is estimated by using a random search approach as described in section 2.3.2. A possible alternative approach is based on Newton's method, a root finding strategy, which iteratively looks for a better approximation of the zeros of a function. In this case, it is necessary to look for the zero of eq. (11), knowing that the zero of the derivative of a function corresponds to a local stationary point (which is unique, if the log-likelihood in (5) is convex). This technique, anyway, requires computing multiple times the first and second derivatives of eq. (5), while exploring the space of possible values of parameter r: it may be computational expensive, and prone to numerical errors, depending of the strategy adopted to implement the numeric approximation of these derivatives [24], and therefore here it was decided to adopt the first, sampling-based, strategy.

Conventional EM-based algorithms allow to avoid the need for data pre-correction by including into the reconstruction process an estimate of all the factors that may alter the statistical distribution of the data [13,14]. However, often these methods tend to be biased, especially in regions with low activity and higher noise [32]. Moreover, a problem common to all ML methods in PET is ill-conditioning, i.e. the solutions are sensitive to small changes in the data and this leads to estimates with high variance. This ill-conditioning is seen in practice as high spatial variance in the ML images, especially for high iteration numbers of the MLEM or OSEM algorithms [33]. This is an important aspect to consider, especially for cold regions and/or dynamic PET data reconstruction [34]: bias and variability of reconstructed data can lead to an incorrect activity evaluation and to erroneous kinetic modelling [35].

Several attempts have been made for reducing ill-conditioning on MLEM-based algorithms, by adding regularization terms in the iterative steps [33]. Such constraints perform regional smoothening but while

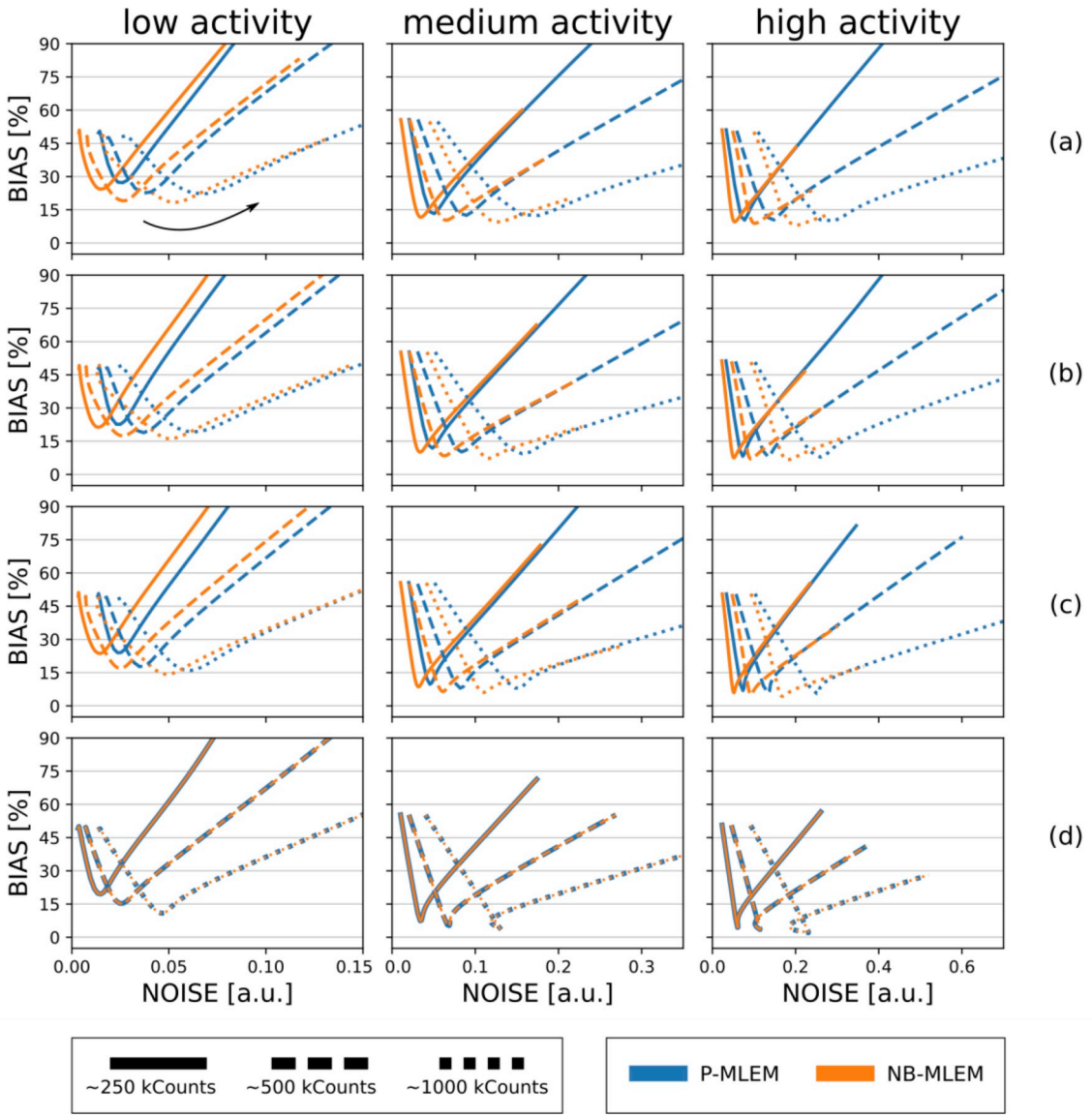

Fig. 5. *Reconstructed images bias vs noise. P-MLEM (blue) and NB-MLEM (orange), for each simulated phantom region, and for different values of the parameters r: a) r = 3.25, b) r = 6.5, c) r = 13.0, and d) r = 1e9. Different line styles are relevant to different sinogram counts (or scan time lengths). The black arrow in the top-left panel shows the direction of increasing number of iterations. The total number of reconstruction iterations was 100, for both the algorithms.*

preserving sharp variations; they are based on the combination of a Poisson likelihood with a series of multi-parametric anato-functional priors of edge total variation (TV)-based methods, which seek to minimize the variations between spatial neighbouring [36,37] taking into account temporal variations in the dynamic PET images [38].

It is worth to note that, pre-correcting data before reconstruction, or performing correction during iterations, are two different approaches to the same problem: to reconstruct PET images from data corrupted by different artefacts. The two approaches have advantages and disadvantages and in literature there are many works in which solutions are proposed that are appropriate to the various problems; in this work we focus on reconstruction methods to be applied after pre-correction, that try to reduce data variability and reconstruction noise. Moreover, especially for kinetic studies, analytical methods like filtered back-projection (FBP) are sometimes still the method of choice despite the usual lower resolution and noise-induced streak artefacts that often corrupt final images [39,40], and it is known that they require pre-correction of measured data in order to perform image reconstruction.

A simulation study to compare the performance of the proposed NB-MLEM algorithm with respect to a conventional Poisson-based MLEM (P-MLEM) method in reconstructing PET data was carried out in the present work. Simulated sinogram data were deliberately distributed according to a NB distribution as consequence of the results obtained by authors in a previous work [9], were it was demonstrated that, performing the pre-correction, the data can be well described as NB-distributed. So, the objective of the present work was to discuss a strategy to improve the quality of the reconstruction by leveraging the knowledge that the data are NB distributed, compared to ignoring this property.

It has been verified that under the assumption that pre-corrected sinograms are NB-distributed, performing image reconstruction using the NB-MLEM method produces images with not only a lower bias but also reduced variance, as it is shown in Fig. 3. As expected, as the iteration number increases, just from visual inspection we can see how the details of the reconstructed image tend to improve for both algorithms, but at the expenses of an increase in noise. However, the proposed NB method is able to limit and slow down the appearance of reconstruction noise corrupting the image.

In Fig. 4, it was shown that, except for the limit case of the quasi-

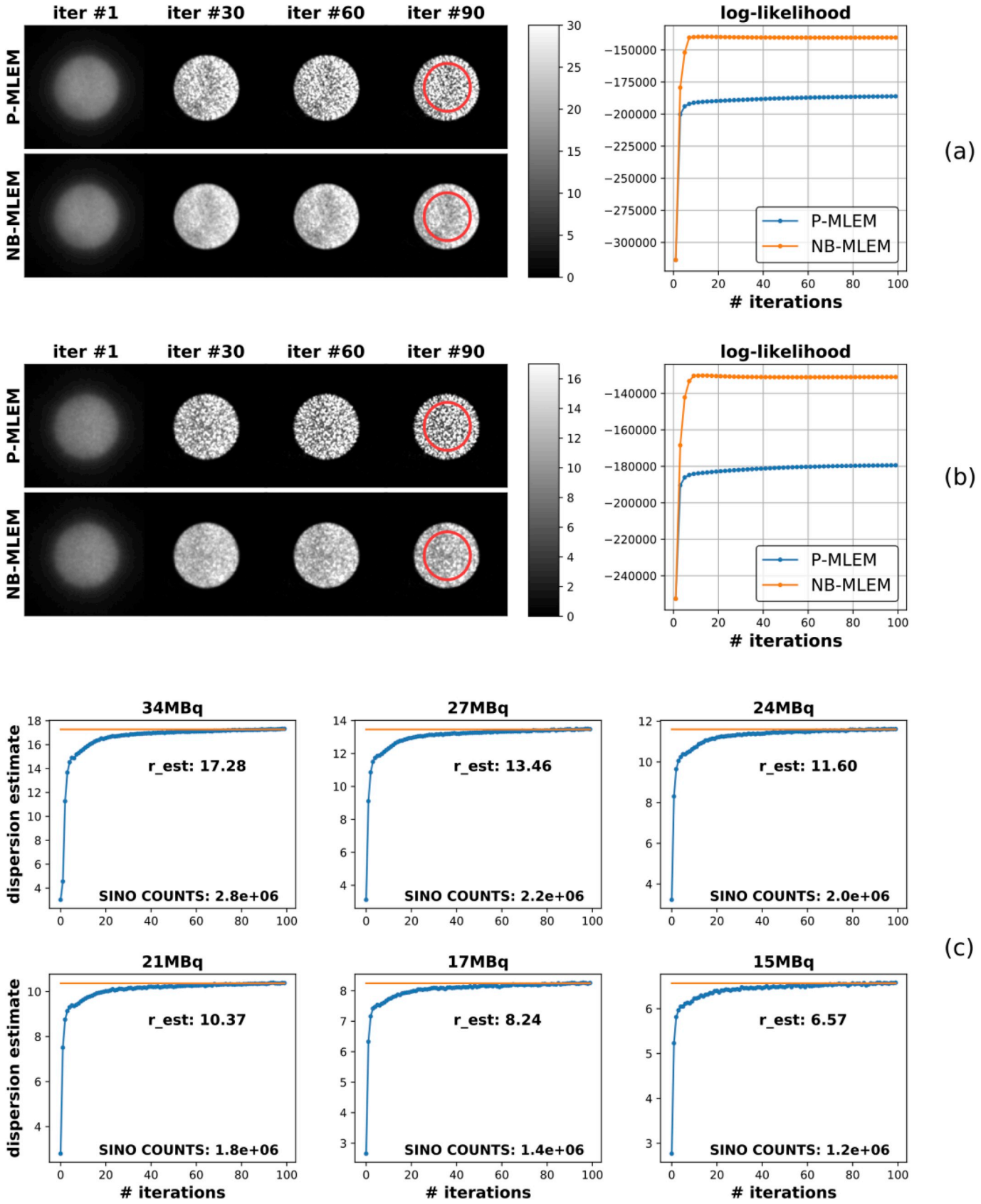

Fig. 6. Experimental phantom reconstruction results. **a)** and **b)** Reconstructed images at different iteration numbers using P-MLEM (top row) and NB-MLEM (bottom row) for the first **(a)** and last **(b)** acquired static scans: reduction in the intensity of the overall emission (expressed as KBq/ml) is due to natural radioactive decay. The relevant log-likelihoods evaluated during the reconstruction of the phantom with the two methods are shown alongside. The red circles show the ROIs used later on to produce the graph in Fig. 7 **c)** parameter r estimated at each iteration by the NB-MLEM algorithm, for each static scan of the real phantom.

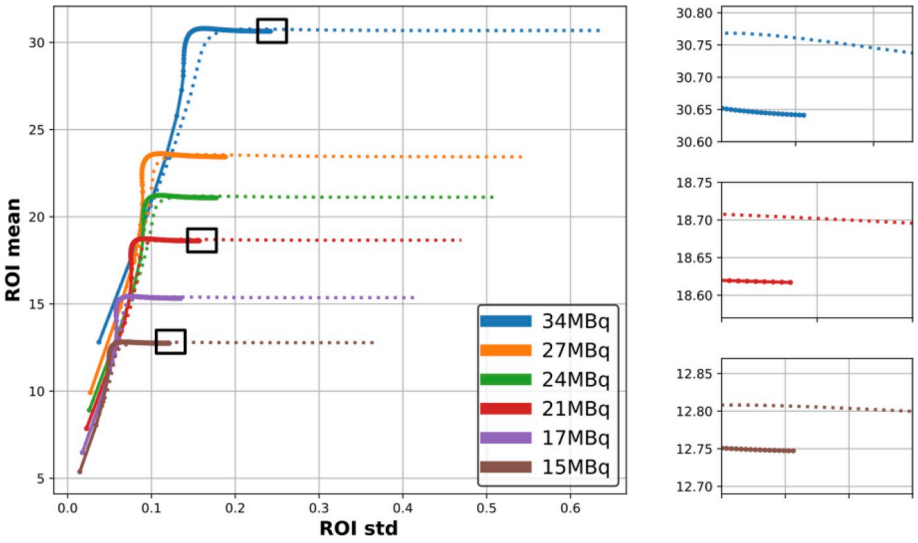

Fig. 7. Plots of ROI mean vs ROI noise, as function of the iteration number for the experimental phantom's reconstructed images. The total number of reconstruction iterations was 100, for both the algorithms. Data are relevant to 6 scan times. Images were obtained by the P-MLEM (dotted lines) and NB-MLEM (continuous lines) algorithms. Zoomed regions, identified by the black rectangles in the plot, are shown on the right.

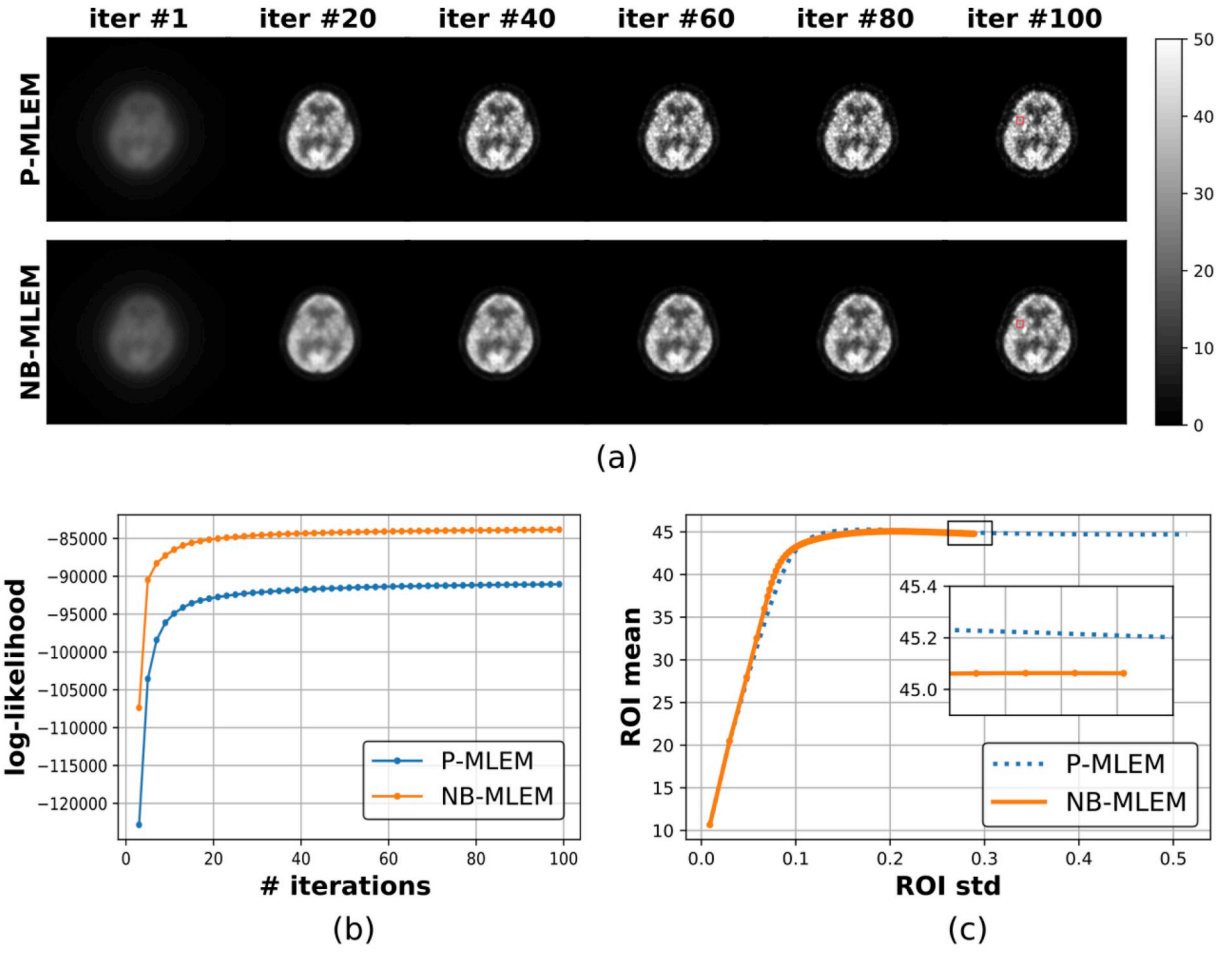

Fig. 8. Real human brain data reconstruction results. **a)** Reconstructed images at different iteration numbers (1,20,40,60,80) using P-MLEM (top row) and NB-MLEM (bottom row). **b)** log-likelihood evaluated during the reconstruction, using both methods. **c)** ROI mean vs ROI noise, as function of the iteration number. Zoomed region of the plot is also shown. The selected ROI covers a gray-matter region of the brain, and it is shown on the last column of **a)**.

Poisson condition ($r = 1e9$), the parameter estimate approaches the true value as the number of iterations increases. For each simulated value of the dispersion parameter, the number of iterations required to obtain a good estimate rises when dealing with higher numbers of total sinogram counts. Increasing the true value of the parameter r (i.e. reproducing a condition of lower level of data overdispersion) the estimate needs a fewer number of iterations to reach a stable convergence, up to the limit case of $r \to \infty$ where the final average value is found since the very beginning.

A few interesting considerations may arise from Fig. 4. The first one is related to the quasi-Poisson condition (last plot on the right, in Fig. 4), in which the parameter r is clearly overestimated. This is probably related to the random search strategy we chose to adopt. This last case simulates a condition with no over-dispersion (i.e. with respect to eq. (2) r tending to infinity and $\alpha \cong 0$ were approximated): sampling the log-likelihood in eq. (5) on a certain search space as described in Section 2.3.2 resulted in an estimate of the r parameter close to the prefixed upper-bound (e.g. ~$2e9$), which is the best approximation of $r \to \infty$ that can be achieved. The numerical strategy adopted in this work to estimate the dispersion parameter seems unable to discriminate very low levels of overdispersion: while this may be solved by designing a different algorithm for the estimate of parameter r, we believe that if we are working in a condition of quasi-Poisson distribution of the data (which is a boundary condition of the problem we want to address), such a small estimation error (i.e. considering that in image update we use $\alpha = 1/r \propto 1e-9$) won't affect the final result of image reconstruction.

Furthermore, the number of iterations required to obtain a good estimate rises when working with higher numbers of total sinogram counts, irrespectively of the true degree of over-dispersion. This might be due to the difficulty of distinguish between a high-mean-high-variance Poisson process, and the presence of actual data over-dispersion. It is possible that different strategies to estimate the dispersion parameter may attenuate this problem, too, but it is also interesting to note how the proposed NB-MLEM algorithm tends to work best with low-counts data, which is often the most common scenario when working with emission imaging data.

In Fig. 5, it can be noted that the images reconstructed using NB-MLEM algorithm (orange lines) achieve a slightly lower bias and noise than the ones obtained with a standard P-MLEM (blue lines), for every combination of sinogram total counts and $r$value. The condition of $r = 1e9$ (last row of Fig. 5) is the only one in which the bias-noise curves overlap: this is an expected result, as for very high r (or low α) the NB-MLEM algorithm approximates the Poisson emission condition (i.e. eq. (10) converges to standard P-MLEM, as discussed in Section 2.3.1) where the P-MLEM algorithm behaves at its best.

As expected, for increasing activity, i.e. moving from left to right subplots in Fig. 5, the bias reduces for both the algorithms, but for NB-MLEM it maintains its minimum value, also when the noise starts to increase. This supports the idea that the quantification of the degree of over-dispersion during reconstruction helps NB-MLEM to reduce both bias and noise with respect to P-MLEM algorithm.

From Fig. 5, it can be also noticed that images reconstructed with the NB-MLEM algorithm have a slower noise increase as the number of iterations increases if compared to P-MLEM images, where the impact of a too great number of iterations on image quality is significant. A possible explanation of this behavior could be that, while working with over-dispersed data, conventional P-MLEM tries to describe data statistics with only one parameter (i.e. mean equal to variance): this may result in higher noise whether the scan time or phantom's emission activity is increased, as both changes affect the mean of the data. In contrast, the parameter r of NB-MLEM is able to capture the degree of over-dispersion in raw data, allowing the reconstruction noise to be almost independent from scan length or injected activity.

In the present work, the study of the optimal number of iterations for the algorithm has not been investigated in detail. Indeed, it should be noted that all ML-based algorithms are often early stopped in practice to avoid (noisy) data overfitting. However, in this work we wanted to show that, even if without considering the optimal stopping condition, the NB algorithm has the ability to generate images with less bias and noise than the more conventional P-MLEM algorithm in almost every case (see Fig. 5).

The proposed NB-MLEM reconstruction algorithm was also tested on a real cylindrical phantom. Working with a real physical system, we did not have the possibility to check all the combinations of injected dose and dispersion factor explored in simulation, mainly because in a real environment the deviation of the raw data from a Poisson distribution is a consequence of the pre-correction operations, and the control on the impact of these steps on the dispersion factor (which, therefore, needs to be estimated from data) is not possible. Acquisition and generation of pre-corrected raw data for different emission activity levels were performed, to compare NB-MLEM and P-MLEM reconstruction at different count rates, as done in the simulation. The choice of a uniform phantom allowed to better control the experimental setup, and to produce different combinations of emission activity and statistical properties.

The experimental study confirmed what was observed in the simulation: in Fig. 6a it can be seen that, starting from a rough and smooth approximation, both algorithms improve the estimate of the activity image, adding details and increasing definition and resolution; using too many iterations, however, causes a rapid increase in reconstruction noise, which corrupts the final result. Again, NB-MLEM seems able to reduce this effect, thanks to a better characterization of the statistical properties of the raw data via proper fitting of the overdispersion parameter. Fig. 6c shows that, as in the simulation, a certain number of iterations is needed to obtain a good approximation of the dispersion parameter, leading to a delay of the achievement of the minimum bias value. On the contrary, wrongly assuming as equal to zero the value of the over-dispersion (i.e. approximating over-dispersed data with a Poisson distribution when using P-MLEM for reconstruction) has a huge impact on the quality of the resulting images.

Comparing the results obtained for different tracer concentrations in the experimental phantom, it can be observed, as expected, how higher concentrations produce higher count rates and, in general, higher variability in reconstructed voxel values. Moreover, looking at the combination of total sinogram counts and estimated dispersion parameter r from experimental phantom data (see Fig. 6c), it can be argued that there should probably be a relationship between the level of over-dispersion introduced by the operations of sinogram pre-correction and the emission count rate. In the simulation study many combinations of injected activity and dispersion parameter were tested, but from the experimental data, it can be argued that not all of them are likely to be legitimate. A more in-depth study is planned for a future work, involving a properly designed phantom study which could highlight some properties of the data that can be exploited to obtain better and faster estimates of the over-dispersion of the pre-corrected data.

Looking at trends of ROI mean vs ROI noise plots as function of the iteration number (Fig. 7), it can be noted that, at fixed iteration number, the NB-MLEM reaches noise values much lower than P-MLEM, and that the estimated mean values are higher in P-MLEM, probably due to the presence of some bias: this is hard to prove, given the lack of knowledge about the true emission value for real data, but it seems to support and to be consistent with the results of the simulation study, both in terms of accuracy of the estimate of r itself (Fig. 4) and of the optimal trade-off between bias and noise (Fig. 5). Given the number of measured counts (>1E6) and r values (between 6.5 and 13) estimated from the phantom data, these experimental results should be compared with the simulation results shown in Fig. 5 b and c, dotted lines.

To assess the performance of the proposed algorithm in an even more complex condition, a real human brain dataset was analysed. Reconstructed images at different iterations shown in Fig. 8a confirm what already seen in the simulation and phantom data: by increasing the iteration number the images become more detailed, but with increasing noise, with the P-MLEM producing reconstructed images which are

noisier than those of NB-MLEM. This is also demonstrated in the ROI mean vs ROI noise plot in Fig. 8c, relevant to a gray-matter region. Moreover, from Fig. 8c it can be seen, again, that the ROI mean evaluated by using the P-MLEM algorithm maintains slightly higher values than the ones obtained with the NB-MLEM algorithm, confirming what also seen in the experimental phantom results (see Fig. 7).

The results obtained in the present work are very promising, and they can be considered as a starting point for further improvements, since there are some weaknesses that should be addressed, and their overcoming could improve the performance of the method. The followings are some aspects that need further analysis.

In the proposed NB-MLEM algorithm we used a global over-dispersion factor, that is a unique value for all sinogram data. Ideally, the appearance of an over-dispersion behaviour in counts data should be described as a local effect, as the pre-correction operations are applied independently for each sinogram bin. Nonetheless, our previous studies aimed at characterizing the statistical properties of pre-corrected counts, using either a Conway-Maxwell-Poisson [10] or a NB distribution [9], gave us reason to believe that it could be reasonable to also use a global over-dispersion factor as a way to describe the overall change of sinogram statistic caused by pre-correction.

The proposed NB-MLEM algorithm, including in the iterative image-update algorithm also the estimation of the dispersion-related parameter, tries to improve the trade-off between bias and noise, when compared to other algorithms that do multiplicative update of positive values with positive factor and that assume no over-dispersion of pre-corrected data, such as P-MLEM. In order to further reduce the bias, especially when dealing with low counts sinograms, it would be interesting to evaluate a modified version of the NB-MLEM algorithm which could take into account the presence of negative values in pre-corrected count data. In fact, it is known that, for low count data, pre-correction operations may produce negative values in the sinogram. New iterative algorithms [32,41], allowing for negative values also in the reconstructed images, have proven to be able to achieve lower biases than conventional MLEM or OSEM in this specific condition. It is the scope of a future work to investigate the possibility of extending the algorithm discussed in this paper, as an example, using a method similar to the one proposed by Li et al. [42], distinguishing the type of update equation at each iteration, depending on whether the sinogram values are positive or not; this would likely further reduce the bias in the reconstructed data.

As a concluding remark, we would like to point out how, in general, the exact solution of the P-MLEM algorithm is rarely used in a clinical setting. Even for un-corrected raw sinogram data, it tends to converge towards very noisy solutions, similarly to what shown in Fig. 5. For this reason, a steadily growing field of research is focused on finding novel strategies to improve the quality of the resulting images, in terms of noise reduction or resolution enhancement. They can be found in every commercial and research system, making their reconstruction software rather different from the core P-MLEM algorithm from which they originated. In this work, we showed how the NB-MLEM algorithm could be better suited to deal with pre-corrected count data, and that it can be seen as a generalization of the P-MLEM, thus configuring itself as an alternative to it, under specific conditions. It is reasonable to think that most of the techniques to improve the quality of the reconstructed images built on top of the core P-MLEM could be extended also to work with the NB-MLEM. An example of this is the leveraging of regularization methods, which have been widely discussed in the literature about Poisson MLEM-based iterative algorithms: given the similarity of the mathematical form of the update equation, it should be easy enough to adapt them to work also within an NB-MLEM reconstruction in order to further improve the convergence of the algorithm. Further studies are planned to verify this assumption.

5. Conclusion

In this work, an NB-based MLEM reconstruction algorithm is described and applied on simulated and experimental PET data. It is based on iteratively estimating the two parameters of the NB distribution, the activity image x and the data dispersion factor α, according to the MLEM strategy. For the property of NB distribution, for $\alpha = 0$ the proposed algorithm behaves like the conventional MLEM algorithm for Poisson distributed data (P-MLEM), and therefore it can be seen as a generalization of it.

Following the hypothesis of modeling pre-corrected PET projection data with an NB distribution, the proposed NB-MLEM algorithm can be used for image reconstruction: the additional evaluation of the parameter r (i.e. $r = 1/\alpha$) after each iteration leads to a more accurate final image, thanks to a better modeling of the statistical properties of the data. With respect to the P-MLEM method, the estimate of the dispersion parameter requires therefore an additional optimization step to be performed. The simulation study performed in this work showed how the suggested random search approach used to estimate r is accurate enough, for any value of r.

In conclusion, the proposed NB-MLEM algorithm resulted to be a viable method for PET image reconstruction starting from pre-corrected data, which exhibits statistical behavior that deviates from the Poisson distribution. There are still a few aspects that would require further investigation, but the results achieved in this first study make it possible to see it as a promising starting point for future improvements.

Declaration of competing interest

None declared.

References

[1] L.A. Shepp, Y. Vardi, Maximum likelihood reconstruction for emission tomography, IEEE Trans. Med. Imaging 1 (1982) 113–122, https://doi.org/10.1109/TMI.1982.4307558.
[2] K. Lange, R. Carson, EM reconstruction algorithms for emission and transmission tomography, J. Comput. Assist. Tomogr. 8 (1984) 306–316.
[3] H.M. Hudson, R.S. Larkin, Accelerated image reconstruction using ordered subsets of projection data, IEEE Trans. Med. Imaging 13 (1994) 601–609, https://doi.org/10.1109/42.363108.
[4] D.F. Yu, J.A. Fessler, Mean and variance of coincidence counting with deadtime, Nucl. Instrum. Methods Phys. Res. Sect. Accel. Spectrometers Detect. Assoc. Equip. 488 (2002) 362–374, https://doi.org/10.1016/S0168-9002(02)00460-6.
[5] Sangtae Ahn, J.A. Fessler, Statistical emission image reconstruction for randoms-precorrected PET scans using negative sinogram values, IEEE, 2004, pp. 3062–3066, https://doi.org/10.1109/NSSMIC.2003.1352544.
[6] B. Guerin, G.E. Fakhri, Realistic PET Monte Carlo simulation with pixelated block detectors, light sharing, random coincidences and dead-time modeling, IEEE Trans. Nucl. Sci. 55 (2008) 942–952, https://doi.org/10.1109/TNS.2008.924064.
[7] S.R. Cherry, J.A. Sorenson, M.E. Phelps, Physics in Nuclear Medicine, fourth ed., Elsevier/Saunders, Philadelphia, 2012.
[8] A. Teymurazyan, T. Riauka, H.-S. Jans, D. Robinson, Properties of noise in positron emission tomography images reconstructed with filtered-backprojection and row-action maximum likelihood algorithm, J. Digit. Imaging 26 (2013) 447–456, https://doi.org/10.1007/s10278-012-9511-5.
[9] M.F. Santarelli, V. Positano, L. Landini, Measured PET data characterization with the negative binomial distribution model, J. Med. Biol. Eng. 37 (2017) 299–312, https://doi.org/10.1007/s40846-017-0236-2.
[10] M.F. Santarelli, D. Della Latta, M. Scipioni, V. Positano, L. Landini, A Conway-Maxwell-Poisson (CMP) model to address data dispersion on positron emission tomography, Comput. Biol. Med. 77 (2016) 90–101, https://doi.org/10.1016/j.compbiomed.2016.08.006.
[11] H. Zaidi (Ed.), Quantitative Analysis in Nuclear Medicine Imaging, Springer US, 2006. https://www.springer.com/gp/book/9780387238548. (Accessed 16 July 2019).
[12] M. Dawood, X. Jiang, K. Schäfers, Correction Techniques in Emission Tomography, CRC Press, 2012.
[13] C. Comtat, F. Bataille, C. Michel, J.P. Jones, M. Sibomana, L. Janeiro, R. Trebossen, OSEM-3D reconstruction strategies for the ECAT HRRT. Nucl. Sci. Symp. Conf. Rec., IEEE, 2004, pp. 3492–3496, https://doi.org/10.1109/NSSMIC.2004.1466639. IEEE, 2004.
[14] M.E. Casey, Point Spread Function Reconstruction in PET, Knoxv. USA Siemens Med. Solut. Inc., 2007, pp. 1–7.

[15] S. Ahn, J.A. Fessler, Emission image reconstruction for randoms-precorrected PET allowing negative sinogram values, IEEE Trans. Med. Imaging 23 (2004) 591–601, https://doi.org/10.1109/TMI.2004.826046.
[16] C.C. Watson, New, faster, image-based scatter correction for 3D PET, IEEE Trans. Nucl. Sci. 47 (2000) 1587–1594, https://doi.org/10.1109/23.873020.
[17] S.J. Clark, J.N. Perry, Estimation of the negative binomial parameter κ by maximum quasi -likelihood, Biometrics 45 (1989) 309–316, https://doi.org/10.2307/2532055.
[18] B.-J. Park, D. Lord, Adjustment for maximum likelihood estimate of negative binomial dispersion parameter, Transp. Res. Rec. J. Transp. Res. Board. 2061 (2008) 9, https://doi.org/10.3141/2061-02.
[19] J.O. Lloyd-Smith, Maximum likelihood estimation of the negative binomial dispersion parameter for highly overdispersed data, with applications to infectious diseases, PLoS One 2 (2007) e180, https://doi.org/10.1371/journal.pone.0000180.
[20] Y. Zhang, Z. Ye, D. Lord, Estimating dispersion parameter of negative binomial distribution for analysis of crash data: bootstrapped maximum likelihood method, Transp. Res. Rec. J. Transp. Res. Board. 2019 (2007) 15–21, https://doi.org/10.3141/2019-03.
[21] Y. Vardi, L.A. Shepp, L. Kaufman, A statistical model for positron emission tomography, J. Am. Stat. Assoc. 80 (1985) 8–20, https://doi.org/10.2307/2288030.
[22] J.-B. Hiriart-Urruty, C. Lemarechal, Convex Analysis and Minimization Algorithms I: Fundamentals, Springer-Verlag, Berlin Heidelberg, 1993. http://www.springer.com/la/book/9783540568506. (Accessed 30 January 2019).
[23] A. Sawatzky, C. Brune, T. Kösters, F. Wübbeling, M. Burger, EM-TV methods for inverse problems with Poisson noise, in: M. Burger, A.C.G. Mennucci, S. Osher, M. Rumpf (Eds.), Level Set PDE Based Reconstr. Methods Imaging Cetraro Italy 2008 Ed. Martin Burger Stanley Osher, Springer International Publishing, Cham, 2013, pp. 71–142, https://doi.org/10.1007/978-3-319-01712-9_2.
[24] W.W. Piegorsch, Maximum likelihood estimation for the negative binomial dispersion parameter, Biometrics 46 (1990) 863, https://doi.org/10.2307/2532104.
[25] Z. Ugray, L. Lasdon, J. Plummer, F. Glover, J. Kelly, R. Martí, Scatter search and local NLP solvers: a multistart framework for global optimization, Inf. J. Comput. 19 (2007) 328–340, https://doi.org/10.1287/ijoc.1060.0175.
[26] S. Pedemonte, C. Catana, K.V. Leemput, An inference language for imaging. Bayesian Graph. Models Biomed. Imaging, Springer, Cham, 2014, pp. 61–72, https://doi.org/10.1007/978-3-319-12289-2_6.
[27] S. Pedemonte, N. Fuin, M. Scipioni, C. Catana, Occiput.io. http://tomographylab.scienceontheweb.net/, 2017.
[28] C.A. Bouman, K. Sauer, A unified approach to statistical tomography using coordinate descent optimization, IEEE Trans. Image Process. 5 (1996) 480–492, https://doi.org/10.1109/83.491321.
[29] M. Yavuz, M. Yavuz, J.A. Fessler, Statistical image reconstruction methods for randoms-precorrected PET scans, Med. Image Anal. 2 (1998) 369–378, https://doi.org/10.1016/S1361-8415(98)80017-0.
[30] J.A. Fessler, Penalized weighted least-squares image reconstruction for positron emission tomography, IEEE Trans. Med. Imaging 13 (1994) 290–300, https://doi.org/10.1109/42.293921.
[31] C. Comtat, P.E. Kinahan, M. Defrise, C. Michel, D.W. Townsend, Fast reconstruction of 3D PET data with accurate statistical modeling, IEEE Trans. Nucl. Sci. 45 (1998) 1083–1089, https://doi.org/10.1109/23.681983.
[32] K. Van Slambrouck, S. Stute, C. Comtat, M. Sibomana, F.H.P. van Velden, R. Boellaard, J. Nuyts, Bias reduction for low-statistics PET: maximum likelihood reconstruction with a modified Poisson distribution, IEEE Trans. Med. Imaging 34 (2015) 126–136, https://doi.org/10.1109/TMI.2014.2347810.
[33] J. Qi, R.M. Leahy, Iterative reconstruction techniques in emission computed tomography, Phys. Med. Biol. 51 (2006) R541–R578.
[34] M.F. Santarelli, N. Vanello, M. Scipioni, G. Valvano, L. Landini, New imaging frontiers in cardiology: fast and quantitative maps from raw data, Curr. Pharmaceut. Des. (2017), https://doi.org/10.2174/1381612823666170328143348.
[35] M. Scipioni, M.F. Santarelli, V. Positano, L. Landini, The influence of noise in dynamic PET direct reconstruction. XIV Mediterr. Conf. Med. Biol. Eng. Comput., Springer, Cham, 2016, pp. 308–313, https://doi.org/10.1007/978-3-319-32703-7_61, 2016.
[36] A. Mehranian, M.A. Belzunce, F. Niccolini, M. Politis, C. Prieto, F. Turkheimer, A. Hammers, A.J. Reader, PET image reconstruction using multi-parametric anato-functional priors, Phys. Med. Biol. 62 (2017) 5975–6007, https://doi.org/10.1088/1361-6560/aa7670.
[37] M. Burger, J. Müller, E. Papoutsellis, C.B. Schönlieb, Total variation regularization in measurement and image space for PET reconstruction, Inverse Probl. 30 (2014) 105003, https://doi.org/10.1088/0266-5611/30/10/105003.
[38] Z. Zhang, H. Liu, Nonlocal total variation based dynamic PET image reconstruction with low-rank constraints, Phys. Scr. 94 (2019), 065202, https://doi.org/10.1088/1402-4896/ab0854.
[39] F.H.P. van Velden, R.W. Kloet, B.N.M. van Berckel, S.P.A. Wolfensberger, A. A. Lammertsma, R. Boellaard, Comparison of 3D-OP-OSEM and 3D-FBP reconstruction algorithms for High-Resolution Research Tomograph studies: effects of randoms estimation methods, Phys. Med. Biol. 53 (2008) 3217, https://doi.org/10.1088/0031-9155/53/12/010.
[40] A. Reilhac, S. Tomeï, I. Buvat, C. Michel, F. Keheren, N. Costes, Simulation-based evaluation of OSEM iterative reconstruction methods in dynamic brain PET studies, Neuroimage 39 (2008) 359–368, https://doi.org/10.1016/j.neuroimage.2007.07.038.
[41] H. Lim, Y.K. Dewaraja, J.A. Fessler, A PET reconstruction formulation that enforces non-negativity in projection space for bias reduction in Y-90 imaging, Phys. Med. Biol. 63 (2018) 035042, https://doi.org/10.1088/1361-6560/aaa71b.
[42] Q. Li, R.M. Leahy, Statistical modeling and reconstruction of randoms precorrected PET data, IEEE Trans. Med. Imaging 25 (2006) 1565–1572.